



**Acoustics'08  
Paris**  
June 29-July 4, 2008

[www.acoustics08-paris.org](http://www.acoustics08-paris.org)

## Fan Blade Trailing-Edge Noise Prediction Using RANS Simulations

Yannick Rozenberg<sup>a</sup>, Michel Roger<sup>b</sup> and Stéphane Moreau<sup>c</sup>

<sup>a</sup>ONERA, BP 72 - 29 avenue de la Division Leclerc, 92322 Chatillon Cedex, France

<sup>b</sup>Ecole Centrale de Lyon, 36 Avenue Guy de Collongue, Centre Acoustique, 69134 Ecully, France

<sup>c</sup>Valeo Thermal Systems, rue Louis Normand, 8, 78321 La Verrière, France  
[yannick.rozenberg@onera.fr](mailto:yannick.rozenberg@onera.fr)

An analytical model based on Schlinker & Amiet's work dealing with the trailing-edge noise of a blade has been previously validated thanks to a dedicated experiment on a low speed axial fan. Wall-pressure spectra near the trailing-edge of the blade and at different radii are needed for an accurate prediction. Only experiments and LES simulations are able to provide them. In an industrial context, both methods can not be applied since they are too expensive and time-consuming. To overcome this difficulty, RANS simulations are combined with semi-empirical wall-pressure spectra to obtain the needed input data. The effect of the mean-pressure gradient is taken into account. The model is applied first to the noise radiated by an airfoil placed in the open-jet of an anechoic wind tunnel, then to an automotive cooling fan and finally to an aircraft engine fan. RANS simulations are post-processed to run the analytical model with appropriate input data. The noise predictions are then compared with experimental results.

## 1 Introduction

Considering a single subsonic rotor fan, without any stator, the noise produced by rotating blades can be divided into tonal noise at multiples of the blade passing frequency, due to a stationary inflow distortion, and broadband noise. When the ingested flow is highly disturbed, the latter contribution is mainly generated by the random scattering of incident turbulence. The mechanism for an helicopter rotor has been experimentally investigated and compared with analytical models by Paterson & Amiet [1]. In the absence of upstream disturbances, the rotating blade also radiates self noise due to three mechanisms: the vortices generated at the blade tip, the vortex-shedding behind a blunt trailing edge and the scattering of the turbulent boundary layer past the trailing edge. The present paper deals with the trailing-edge noise, which corresponds to the minimum noise level radiated by rotating blades without any installation effect or tip clearance, in low-turbulence inflow conditions.

The main objective of the present paper is to describe a method for using RANS simulations to calculate trailing-edge noise produced by an airfoil or a fan. An analytical model is first exposed. It assumes the knowledge of input data, such as the wall-pressure statistics in the vicinity of the trailing edge. Some models based on scaling techniques are then presented in section 3. The method is first applied to the noise radiated by an airfoil placed in the open-jet of an anechoic wind tunnel, then to an automotive cooling fan and finally to an aircraft engine fan.

## 2 Trailing-edge noise model

In 1976, Amiet published a trailing-edge noise model [2] based on a previous theoretical method for calculating the far-field noise of an airfoil in an incident turbulent flow [3]. A recent paper by Roger & Moreau [4] extended the model to account for the effects of a finite chord length. The model provides the far-field pressure spectrum at any point:

$$S_{pp}(\vec{x}, \omega) = \left( \frac{\omega c x_3}{2\pi c_0 S_0^2} \right)^2 \frac{L}{2} \left| \mathcal{L} \left( \frac{\omega}{U_c}, \frac{\bar{k} x_2}{S_0} \right) \right|^2 \Phi_{pp}(\omega) l_y(\omega). \quad (1)$$

The observer position is defined by a coordinate system centered at the trailing-edge of the airfoil at the mid-span.  $x_1$  is aligned with the inflow velocity,  $x_3$  is perpendicular to both the trailing edge and  $x_1$ , with  $x_3 = 0^+$  on the suction side. Finally,  $x_2$  is aligned with the trailing edge to obtain a direct system.  $L$  and  $c$

are respectively the span and the chord of the airfoil,  $S_0$  is the corrected distance for convection effects,  $\Phi_{pp}$  the wall pressure spectrum,  $l_y$  the spanwise coherence length and  $U_c$  the convection velocity.  $\mathcal{L} = \mathcal{L}_1 + \mathcal{L}_2$  is the aeroacoustic transfer function where  $\mathcal{L}_1$  is the main term defined by Amiet [2] and  $\mathcal{L}_2$  is the back-scattering correction obtained by Roger & Moreau [4].

The formulation (1) is quite different from the one derived by Amiet. An asymptotic analysis at low Mach number and high frequency highlights the presence of a factor 4 between Amiet's model and Howe's model [5]. The presence of this factor in (1) has been validated by comparison with experimental results on airfoils.

The previous model has been extended by Schlinker & Amiet [6] to a low solidity helicopter rotor blade based on a strip theory. The blade is split into  $n$  segments. The airfoil theory is applied to each segment, assuming that the circular motion is locally tangent to an equivalent translating motion. Considering a blade segment according to the sketch of Fig.1, the single-airfoil formulation 1 gives the radiated sound from one azimuthal location with no relative motion with respect to the observer. The relative motion of the blade is taken into account by adding a Doppler factor expressed by the equation (2) below.

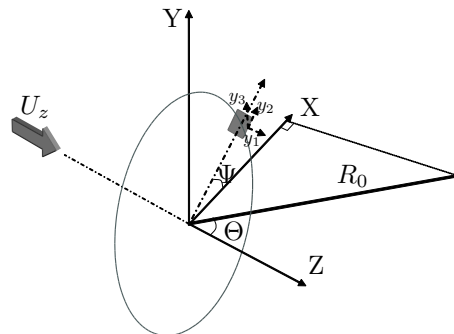


Figure 1: Coordinate system used in the rotating blade model.

The first step consists in calculating the observer coordinates in the reference frame of the appropriate blade segment. The observer position in the moving reference frame is defined by the vector sum  $\vec{y} = \vec{R}_0 - \vec{R}_A$  where  $\vec{R}_A = (0; R; 0)$  denotes the middle of the trailing-edge segment in the  $(y_1; y_2; y_3)$  coordinate system (see Fig.1). Equation (1) gives the sound radiated by the segment, provided the observer coordinates are expressed in the rotating reference frame and the frequency is corrected by the Doppler factor due to the relative motion. The instantaneous emitted frequency  $\omega_e(\Psi)$  at the current

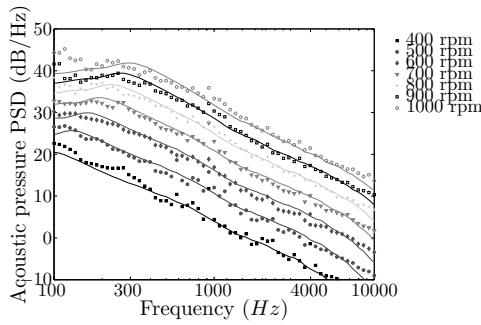


Figure 2: Acoustic pressure PSD in the rotational plane. Experimental (symbols) and analytical (lines) results from a low-speed two-bladed fan. Sensors on the blade measure the wall-pressure fluctuations in the vicinity of the trailing edge.

position  $\Psi = \Omega t$  is related to the received frequency  $\omega$  by [7]:

$$\frac{\omega_e}{\omega} = 1 + \frac{M_t \sin \Psi \sin \Theta}{\sqrt{1 - M_z^2 \sin^2 \Theta}}. \quad (2)$$

where  $M_t$  is the Mach number of the source relative to the observer and  $M_z$  is the axial Mach number. The resulting spectrum must be calculated by averaging over all possible angular locations of the blade segment and by weighting with the Doppler ratio to be physically consistent with the necessary conservation of energy. This yields the following far-field noise PSD for a fan with  $B$  independent blades:

$$S_{pp}(\vec{x}, \omega) = \frac{B}{2\pi} \int_0^{2\pi} \frac{\omega_e(\Psi)}{\omega} S_{pp}^{\Psi}(\vec{y}, \omega_e) d\Psi \quad (3)$$

$S_{pp}^{\Psi}$  is given by the single-airfoil theory where the observer coordinates are defined in the  $(y_1; y_2; y_3)$  coordinate system. The integration over  $\Psi$  is calculated by a recursive Newton-Cotes 8 panel rule. Rozenberg *et al.* [8] provided an experimental validation of the model in the case of a low-speed two-bladed fan. The wall-pressure fluctuations in the vicinity of the trailing-edge are measured by sensors placed in the blade. Fig. 2 compares the far-field noise measured in the rotational plane ( $\Theta = 90^\circ$ ) and the one obtained by the present model with the wall-pressure statistics deduced from the experiment. Provided the wall-pressure statistics is known, the model is able to predict with accuracy the far field noise. The main objective of the paper is to show how these input data can be obtained using RANS simulations.

### 3 Wall-pressure statistics models

The wall-pressure statistics is the main Amiet's model input data. The turbulent boundary-layer is considered as the hydrodynamic excitation and passing the trailing edge, the reorganization of the pressure field induces acoustic radiation. In the present model, the convection velocity, the spanwise coherence length and the wall-pressure spectra just upstream of the trailing edge are needed. The convection velocity is classically taken as

$U_c = \alpha U_e$  with  $0.6 < \alpha < 0.8$ . The average value of  $\alpha = 0.7$  will be used in the following sections. The spanwise coherence length can be deduced from Corcos' model [9]:

$$l_y(\omega) = \frac{bU_c}{\omega}. \quad (4)$$

The constant  $b$  has to be fitted with experimental results. It has been found to be equal to 1.4 for a turbulent boundary layer over a flat plate with no pressure gradient [9]. In the case of a curved surface such as an airfoil or a blade, this value can be slightly modified. It has been found to vary between 1.2 and 1.7 in different airfoil experiments [10]. The value of 1.4 is accepted as a good mean value.

The far-field PSD is directly proportional to the wall-pressure PSD. As the turbulent boundary layer is characterized by a large range of relevant length, velocity and pressure scales, numerous semi-empirical models have been developed. A two-layer model is widely used to scale the turbulent boundary layer. The nearest flow to the wall, called the viscous sub-layer, provides a first set of length, velocity and pressure scales; the outer layer, a second one. Based on this description, Keith *et al.* [11] compared the wall-pressure spectra from various experiments in a normalized form. The high-frequency range of the pressure spectra collapses when it is normalized by inner-layer scales, such as the wall shear stress  $\tau_w$  for the pressure scale and  $\nu/u_\tau^2$  for the timescale, with  $\nu$  the kinematic viscosity and  $u_\tau$  the friction velocity. For low frequencies, a collapse is observed with outer-layer scaling, such as the velocity at the boundary layer edge  $U_e$ , the boundary-layer thickness  $\delta$  or the boundary-layer displacement thickness  $\delta^*$ . Based on this description, three models are briefly reviewed. Combined with a RANS simulation providing the mean field, they give the wall-pressure spectra needed in the equation (1). The single-sided convention is used:  $\overline{p^2} = \int_0^\infty \Phi_{pp}(\omega) d\omega$ .

#### 3.1 Schlinker & Amiet's model

Willmarth & Roos [12] have collected experimental wall-pressure fluctuations beneath a turbulent boundary layer. Based on these data, Schlinker & Amiet [6] proposed an analytical formulation using the outer variables:

$$\frac{\Phi_{pp}(\omega)}{\rho_0^2 \delta^* U_e^3} = 2.10^{-5} \frac{F(\tilde{\omega})}{2}, \quad (5)$$

with

$$F(\tilde{\omega}) = (1 + \tilde{\omega} + 0,217\tilde{\omega}^2 + 0,00562\tilde{\omega}^4)^{-1},$$

where  $\tilde{\omega} = \omega \delta^* / U_e$ . Since the previous model is defined for a zero pressure gradient flat plate, Schlinker & Amiet [6] proposed a correction function  $DIFF(\tilde{\omega})$  for airfoil and blade trailing-edge noise.

#### 3.2 Goody's model

Goody's objective is to take into account the effect of the Reynolds number using an empirical approach [13]. Based on Chase-Howe's model [14, 15] and the experimental results of seven research groups. The only effect

of Reynolds number on the shape of the wall-pressure spectrum is to increase the size of the overlap range. The final form of the semi-empirical model is:

$$\frac{\Phi_{pp}(\omega)U_e}{\tau_w^2\delta} = \frac{C_2(\omega\delta/U_e)^2}{\left[(\omega\delta/U_e)^{0.75} + C_1\right]^{3.7} + [C_3(\omega\delta/U_e)]^7}, \quad (6)$$

with  $C_1 = 0,5$ ,  $C_2 = 3,0$  and  $C_3 = 1,1R_T^{-0.57}$ .  $R_T = (\delta/U_e)/(\nu/u_\tau^2) = (u_\tau\delta/\nu)\sqrt{C_f/2}$  is the ratio of the outer-layer-to-inner-layer timescale characterizing the Reynolds number effect.

### 3.3 Mean-pressure gradient model

The effect of an adverse pressure-gradient on the wall-pressure spectra has been observed experimentally by Schloemer [16] and numerically by Na [17]. The normalized wall-pressure spectra can be increased by 10 dB. This effect has to be taken into account. Based on Goody's model, an empirical improved model has been proposed by Rozenberg [18]:

$$\frac{\Phi_{pp}(\omega)U_e}{\tau_w^2\delta^*} = \frac{0.78(1.8\Pi\beta_C + 6)\left(\frac{\omega\delta^*}{U_e}\right)^2}{\left[\left(\frac{\omega\delta^*}{U_e}\right)^{0.75} + C'_1\right]^{3.7} + \left[C'_3\left(\frac{\omega\delta^*}{U_e}\right)\right]^7}, \quad (7)$$

with  $C'_1 = 0.105$  and  $C'_3 = 3.76R_T^{-0.57}$ .  $\beta_C = (\theta/\tau_w)(dp/dx)$  is known as Clauser's parameter [19] and  $\Pi$  is the parameter of the wake's law defined by Coles [20] and obtained by solving:

$$2\Pi - \ln(1 + \Pi) = \frac{\kappa U_e}{u_\tau} - \ln\left(\frac{\delta^* U_e}{\nu}\right) - \kappa C - \ln \kappa, \quad (8)$$

with  $\kappa = 0,41$  and  $C = 5,1$ .

## 4 Application to a test airfoil

The test airfoil is an industrial airfoil designed for automotive engine cooling fans. It has been placed in the nozzle exit of an open-jet wind tunnel with a high angle of attack ( $20^\circ$ ) and an inflow velocity  $U_0 = 16$  m/s. The experimental set-up and results have been presented by Rozenberg *et al.* [21]. The RANS simulation is presented in the following section and the wall-pressure models of section 3 coupled with Amiet's trailing edge model are then applied to the present test-case.

### 4.1 RANS simulation and validation

A 2D RANS simulation is carried out thanks to Fluent 6.2. The airfoil and the nozzle exit are simulated using a wall boundary condition. The whole anechoic chamber is meshed with 120 000 elements. A  $k - \omega$  SST turbulence model is applied since it is able to capture the laminar separation bubble near the leading-edge on the suction side. The mesh is fine enough to avoid the use of wall functions ( $y^+ < 1$ ). The simulation is validated by comparing with the experiment the mean-pressure distribution on the airfoil and the velocity profile just downstream of the airfoil (see Fig.3). The turbulent

boundary-layer is investigated along a normal to the suction side at 90% of chord from the leading edge. The data are sum up in the Table 1. To be efficient, this model requires a fine mesh in order to well reproduce the inner variables, especially the wall-shear stress.

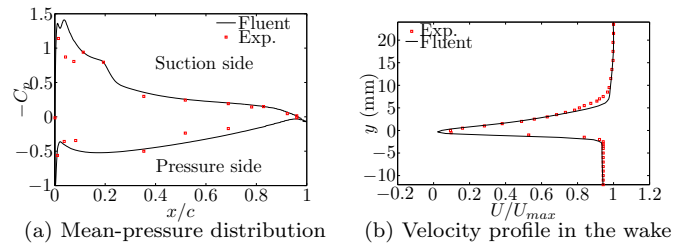


Figure 3: Validation of the airfoil RANS simulation.

$U_e$	$\delta$	$\delta^*$	$\theta$	$\tau_w$	$\tau_{max}$	$\beta_C$	$\Pi$
19.8	3.87	0.992	0.559	0.61	0.75	1.85	1.39

Table 1: Airfoil boundary-layer parameters

### 4.2 Application

Amiet's trailing-edge noise model is applied to the present airfoil. The formulation (1) provides the far-field pressure spectra induced by the turbulent boundary layer past the trailing edge of the airfoil. The aforementioned wall-pressure spectral models are compared to the experimental result in Fig.(4). Schlinker's model and Goody's model predict quite the same pressure spectrum (except at low frequencies) which is underestimated. This underestimation is due to the mean-pressure gradient effect, not taken into account in both spectral models. In contrast, the use of the mean-pressure gradient model in Eq.(1) provides an excellent agreement with the experimental results over the whole range of frequency. Schlinker's model can also be improved by the addition of the *DIFF* function.

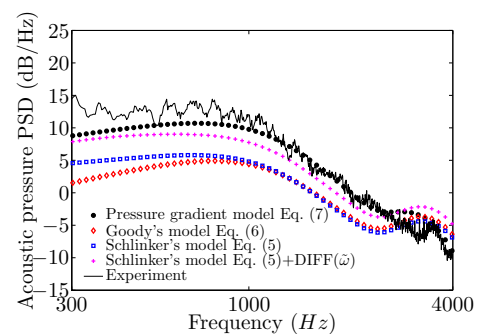


Figure 4: Far-field acoustic spectra in the mid-span plane of the airfoil.

## 5 Application to an automotive cooling fan

The rotating model is applied to a 9-blade fan with a blade-tip radius of 380 mm. The duty point is chosen so that experimental results are available to be compared with the model: a rotational speed  $N = 2400$  rpm and a mass flow rate  $Q = 2262$  m<sup>3</sup>/h. A 3D RANS simulation provides the input data at each strip. The pressure spectra given by the analytical model at different angular positions are then integrated over a semi-spherical surface to be compared to the sound power measured in a reverberant room at the same duty point.

### 5.1 3D RANS simulation and post-processing

A high quality and fine grid (3.6 million nodes) is coupled with CFX-TASCflow to simulate the flow around the fan with the appropriate boundary conditions. The convective terms are discretized with second-order upwind schemes and the other terms with second-order central differences. A  $k - \omega$  SST turbulence model is used.

The wall-pressure statistics are deduced from the simulation thanks to the empirical models. The blade is split into 6 segments which are then considered as rectangular plates with local geometry and orientation. In the middle of the considered segment, the total pressure and velocity profiles are interpolated into a normal to the wall just upstream of the trailing edge on the suction side. The outer and inner turbulent boundary-layer variables are presented in Table (2).

radius (cm)	8.3	10.2	12.0	13.8	15.7	17.5
chord (cm)	5.5	6.5	6.5	6.2	5.9	5.8
$U_e$ (m/s)	9.0	19.0	26.8	32.4	36.2	13.8
$\delta$ (mm)	2.2	2.9	3.1	2.9	2.5	1.0
$\delta^*$ (mm)	1.0	0.5	0.8	0.8	0.7	0.2
$\theta$ (mm)	0.35	0.31	0.43	0.35	0.33	0.11
$\tau_w$ (Pa)	0.83	1.26	2.33	0.96	1.61	1.97
$\beta_C$	1.82	1.65	2.00	3.30	2.90	0.91
$\Pi$	-	-	-	3.82	2.69	-

Table 2: Automotive fan boundary-layer and geometrical parameters

### 5.2 Application

Eq. (3) is applied to the automotive cooling fan at the duty point chosen for simulation. The power spectral density of the acoustic pressure is evaluated at various angular positions and is integrated over a semi-spherical surface since the acoustic radiation at inlet has been measured in a reverberant room. The fan was run in wooden shroud, in a board mounted configuration. Though the board mounted configuration is not the standard sound measurement condition, the tests were run in this manner to isolate fan-only noise. The comparison of the narrow-band and third-octave sound power spectra is presented in Figs.(5) and (6). As in

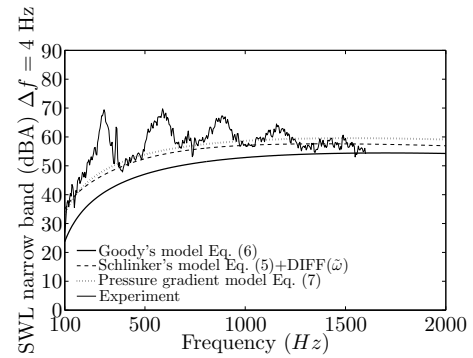


Figure 5: Narrow band inlet sound power spectra from a Valeo engine cooling fan.

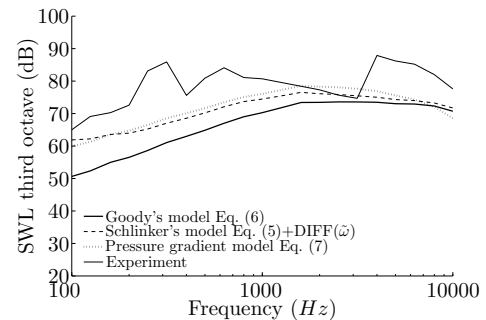


Figure 6: Third-octave inlet sound power spectra from a Valeo engine cooling fan.

the previous section dealing with a 2D experiment, the omission of the mean-pressure gradient leads to underestimate the sound radiated. Goody's model (Eq. (6)) does not take the mean-pressure gradient effect whereas the pressure gradient model (Eq. (7)) and Schlinker's model (Eq. (5)) using the *DIFF* function allow to obtain a good fit between the analytical model and the experiment.

## 6 Application to an aircraft engine fan

The flow around an aircraft engine fan has been obtained by a RANS simulation (elsA) provided by Snecma. Usually, the major broadband noise contribution for a fan is due to the turbulence interaction noise. The fan selected in the present study is known to have an expected strong trailing-edge noise contribution. The post-processing is similar to the one used for the cooling fan. The mesh is not fine enough to compute the  $\Pi$  parameter from the law of the wake. So the pressure gradient model can not be used and only Schlinker's model with the *DIFF* function will be evaluated. The far-field model previously described is applied to a ducted fan. It assumes that the cut-on modes carry the whole energy and it neglects the reflections at the duct ends. A simplified correction is also proposed to model the shielding cascade effect [18].

Fig.(7) compares the analytical model with experimental results for 3 engine speeds. At high frequencies, noise is mainly due to rotor-stator interaction. At low frequencies, the model underpredicts the noise level of

about 5 dB but the variation with both frequency and rotational speed is well reproduced.

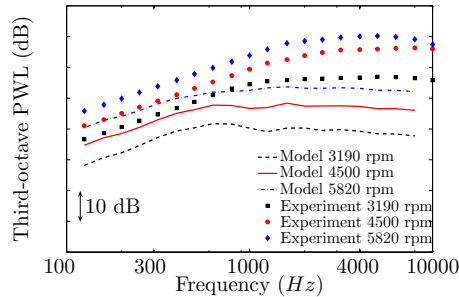


Figure 7: Broadband inlet PWL for an engine fan. Snecma test-case.

## 7 Conclusion

Scaling techniques have been used to provide Amiet's model input data, based on the knowledge of mean flow parameters such as the inner and outer turbulent boundary-layer variables. RANS simulations of a high-loaded airfoil, an automotive cooling fan and an aircraft engine fan have been performed and post-processed to obtain wall-pressure spectra just upstream of the trailing edge. The effect of the mean-pressure gradient on the trailing-edge noise is seen to be of primary importance and the use of appropriate spectral models is needed.

## Acknowledgments

The present work was achieved as a collaboration between Valeo, CETIAT, SNECMA and Ecole Centrale de Lyon. The study was supported by the CIRT (Consortium Industrie-Recherche en Turbomachine), together with the French Ministry of Research. The authors would like to thank Manuel Henner from Valeo and Benoit Farvacque from Snecma for providing the RANS data for automotive cooling fan and aircraft engine fan applications.

## References

- [1] Paterson, R. W. and Amiet, R. K., "Noise of a Model Helicopter Rotor Due to Ingestion of Turbulence," CR - 3213, NASA, (1979)
- [2] Amiet, R. K., "Noise due to turbulent flow past a trailing edge," *J. Sound Vib.* 47, 387–393, (1976)
- [3] Amiet, R. K., "Acoustic radiation from an airfoil in a turbulent stream," *J. Sound Vib.* 41, 407–420, (1975)
- [4] Roger, M. and Moreau, S., "Back-scattering correction and further extensions of Amiet's trailing edge noise model. Part 1: theory," *J. Sound Vib.* 286, 477–506, (2005)
- [5] Howe, M. S., "A review of the theory of trailing-edge noise," *J. Sound Vib.* 61, 437–465, (1978)
- [6] Schlinker, R. H. and Amiet, R. K., "Helicopter Rotor Trailing Edge," CR - 3470, NASA, (1981)
- [7] Amiet, R. K., "Frame of Reference Considerations for the Forward Flight Noise Problem," N212775-1, UARL, (1974)
- [8] Rozenberg, Y., Roger, M., Guédel, A., and Moreau, S., "Rotating Blade Self Noise: Experimental Validation of Analytical Models," No. AIAA-2007-3709, (2007)
- [9] Corcos, G. M., "The structure of turbulent pressure field in boundary-layer flows," *J. Fluid Mech.* 18, 353–378, (1964)
- [10] Roger, M. and Moreau, S., "Broadband Self-Noise from Loaded Fan Blades," *AIAA Journal* 42, 536–544, (2004)
- [11] Keith, W. L., Hurdis, D. A., and Abraham, B. M., "A Comparison of Turbulent Boundary Layer Wall-Pressure Spectra," *J. Fluids Eng.* 114, 338–347, (1992)
- [12] Willmarth, W. W. and Roos, F. W., "Resolution and Structure of the Wall Pressure Field Beneath a Turbulent Boundary Layer," *J. Fluid Mech.* 22, 81–94, (1965).
- [13] Goody, M., "Empirical Spectral Model of Surface Pressure Fluctuations," *AIAA Journal* 42, 1788–1794, (2004)
- [14] Chase, D. M., "Modeling the Wavevector-Frequency Spectrum of Turbulent Boundary Layer Wall Pressure," *J. Sound Vib.* 70, 1980, 29–67, (1980)
- [15] Howe, M. S., *Acoustics of Fluid-Structure Interactions*, Cambridge University Press, (1998)
- [16] Schloemer, H. H., "Effects of Pressure Gradients on Turbulent-Boundary-Layer Wall-Pressure Fluctuations," *J. Acoust. Soc. Am.* 42, 93–113, (1967)
- [17] Na, Y., "Direct numerical simulation of turbulent boundary layers with adverse pressure gradient and separation," PhD dissertation, Stanford University, (1996)
- [18] Rozenberg, Y., "Modélisation analytique du bruit aérodynamique à large bande des machines tournantes: utilisation de calculs moyennés de mécanique des fluides," PhD dissertation, Ecole Centrale de Lyon, (2007)
- [19] Clauser, F. H., "Turbulent Boundary Layers in Adverse Pressure Gradients," *Journal of the Aeronautical Sciences* 21, 91–108, (1954)
- [20] Coles, D., "The law of the wake in the turbulent boundary layer," *J. Fluid Mech.* 1, 191–226, (1956)
- [21] Rozenberg, Y., Roger, M., and Moreau, S., "Effect of Blade Design at Equal Loading on Broadband Noise," No. AIAA-2006-2563, (2006)